7

Liquid Phase Sintering of Fe-Cu-Sn-Pb System for Tribological Applications

Cristina Teisanu
University of Craiova
Romania

1. Introduction

Powder metallurgy technique has become increasingly interesting for engineering parts manufacturers due to its advantages which include high productivity, minimum consumption of raw materials and energy, high efficient use of the initial metals (95–98%), near net shape character and unique capability of porous material production.

This technique results in sintered parts that reach sufficiently high strength properties, for example, similar to cast iron, already at a porosity of 20-15%, and present remarkable physical, chemical and mechanical characteristics, which are determined by their chemical composition and the phase structure as well as the shape and mass distribution of the powder particles. Moreover, by powder metallurgy methods can be obtained materials of virtually any structure, composition and porosity and, thus, any mechanical and service properties.

The performance of equipments, machines, devices and mechanisms is strongly related to their subassemblies and component parts performance. These machines and mechanisms withstand various loads and, thus, complex processes during operating times, but friction, lubrication and wear are among the most frequently met processes.

Sintered antifriction materials are widely used in various tribological applications due to their more homogenous structure and controlled open porosity and grain size, which actually would be impossible to be fabricated by other manufacturing approaches. Besides the high wear resistance and low friction coefficient, sintered antifriction materials have the best possible volume and surface strength, which combines the high strength of the surface layer and the high conformability of the friction pair. Furthermore, they ensure self-lubrication of surfaces with oil from pores, which implies no additional external oil supply. Therefore it is essential to know the actual loading conditions of the part and modify alloying and the treatment conditions of the material on the basis of these conditions.

Sintered iron base antifriction materials were not developed until the last decade because of poor corrosion resistance and antifriction properties. Considering the low cost and

availability of iron powders, the more homogenous structures obtained by sintering and the increased specific load-carrying capacities and sliding rates, the development of the iron base sintered alloys for tribological applications was continuously improved. Additions such as copper, graphite, manganese, lead, antimony and tin to iron have been attempted but improvement in one property was offset by a decrease in other properties (Kostornov & Fushchich, 2007; Kostornov et al., 2007; Shahparast & Davies, 1978; Verghese & Gopinath, 1989). To overcome weaknesses in existing alloy systems and to meet the challenging nature of newer machines, it is important to develop a modified alloy system which can succeed in dealing with these deficiencies, either partially or fully.

Using conventional powder metallurgy techniques the present work is focused on the development of new iron-copper base antifriction materials with different addition elements such as lead, tin and molybdenum disulphide powders. In sintered iron based materials copper has unique properties as an alloying element. In small amounts copper improves strength and rust resistance, and also has a rapid surface diffusion over solid iron (Runfors, 1987, as cited in Boivie, 2000). Therefore, copper is rapidly dissolved into the iron particles, forming a substitution solid solution. Since copper atoms have a larger diameter compared to iron atoms, this causes a distortion in the crystal structure and thus resulting in a swelling effect that is larger than the original copper volume (German, 1985, as cited in Boivie, 2000). Lead exhibits excellent self lubricating property and plays a role of solid lubricant to prevent seizure. In addition, since Pb forms a soft dispersion phase, it has conformability and allows solid matter to be embedded therein. Tin is a key player in antifriction alloys because it can influence both corrosion resistance and fatigue strength and friction and wear properties of these materials can be also improved. During compaction, some phenomena including particle deformation, cold welding at points of contact and interlocking between particles occur. The reasons for non-uniform density distribution are friction between particles and die, and internal friction between powder particles (Sustarsic, 1998). Because of its lamellar structure, MoS_2 is one of the most popular and usable solid lubricants (Hutchings, 1992, as cited in Sustarsic, 1998). It is very important to understand the parameters that control the densification behaviour and the resulting microstructure (grain size and shape, pore size and shape, phase distribution etc.) because of their effect on the physical and mechanical properties of the final product.

Liquid phase sintering, i.e. sintering where a proportion of the material being sintered is in the liquid state, is a common processing technique for a variety of systems, including metal, cermets and ceramics. The sintered material usually consists of grains of one or more solid phases at the sintering temperature intermixed with phase that is liquid at sintering temperature. Liquid phase sintering is one of the most popular methods to enhance the sintering behaviour of a powder material. During liquid phase sintering a liquid phase coexists with a particulate solid at sintering temperature (German, 1996). If the liquid has good wetting properties over the solid particle and there is solid solubility in the liquid, then an enhanced sintering over all wetted surfaces will occur. This enhancement involves growth along the wetted grain boundaries. Thus, grains situated at a free surface will expand in all lateral directions, while the un-wetted free surface is depleted. This can lead to a smoothing effect on the material surface (Park et al, 1986, as cited in Boivie, 2000).

For the most part, in conventional powder metallurgy, liquid phase sintering exhibits sufficient internal force through liquid capillary action on the particulate solid that external forces are not required for the compaction during sintering (German, 1996).

In this study the formation of the liquid phase during sintering process of Fe-Cu-Sn-Pb system was investigated. The liquid phase produced during sintering led to a considerable accurate process and swelling of the sintered compacts was observed and studied. There are many factors that cause dimensional changes and their combined effect make it more difficult to forecast and control these changes. Consequently, in order to avoid subsequent operations such as sizing and machining it is imperative to improve the final dimensional tolerances obtained after sintering (Takata & Kawai, 1995). Therefore, the evaluation of quantitative effects of the dimensional changes of the sintered compacts was also investigated due to variations of the sintering time, temperature and chemical composition.

The material porosity plays an important role in tribological applications for an adequate functioning of the machines and devices. Self-lubricating bearings accomplish superior performance when the porosity level is high, so sufficient oil is accumulated in the pores during inactivity periods and it leaks when the shaft begins rotate in it. Also, the material density plays an important role for self-lubricating bearings for exhibiting good load bearing capacity. Therefore, self-lubricating bearings need to have a high open porosity level for better performance. The porosity due to closed pores shall be reduced, so that density remains high and hence the load bearing capacity of the bearing (Yusof et al., 2006). Among the most important material characteristics required for self-lubricating bearings are identified to be high porosity and reasonably high density. Thus the effect of sintering parameters (temperature and time) and compacting pressure on porosity of the sintered antifriction materials was systematically examined. The mathematical model of the sintering process of the iron-copper base material for tribological applications was developed by establishing the relationship between density of the material and sintering parameters (temperature and time) and the chemical composition.

2. Liquid phase sintering characterization

2.1 Test materials and experimental procedure

The composite materials are made of elemental powders of iron (DP 200HD), electrolytic copper, tin, lead and MoS_2 as solid lubricant. In this study three compositions are considered and labelled as MAS1, MAS2 and MAS2. Their physical characteristics and chemical composition are presented in table 1. Elemental powders were weighed to selected proportions and mixed in a three-dimensional rotating turbula-type device for two hours. Then the powder mixtures were cold compacted in a single-acting hydraulic press using three pressures (350, 500 and 700 MPa) and cylindrical specimens, 10.0 mm in diameter and 7.0 mm in height, were obtained and used for metallographic examination, measurement of green and sintered density, porosity and dimensional change after sintering. Reference densities for the selected compositions were calculated by the rule of mixtures and green and sintered densities were evaluated gravimetrically using Archimedes principle. Volumetric dimensional change of the sintered compacts was calculated and the total porosity of the specimens was evaluated from the difference between the reference density and the measured density.

Composition of the mixtures [wt %]					
	Copper	Tin	Lead	MoS_2	Iron
Composition 1 – MAS1	5	1	2.5	1	bal.
Composition 2 – MAS2	5	1.5	5	1	bal.
Composition 3 – MAS3	5	2.5	7.5	1	bal.
Characteristics of powders					
Particle size [μm]	< 125	< 100	< 100	1 – 5	< 160
Apparent density [g/cm^3]	2.63	3.7	5.63	-	2.92
Flow rate [s/50g]	28	-	-	-	28.1

Table 1. Physical characteristics of powders and alloys composition.

The compacted samples were placed in a tubular furnace with uniform heating zone and sintered at 800°C, 850°C and 900°C for 20, 35 and 50 minutes. The upper limit of the sintering temperature is chosen considering the high evaporability of the lead at temperatures above 900 and for its sweating phenomenon (Baranov et al., 1990).

The sintering process was performed in dry hydrogen atmosphere (dew point of -15 °C) with a flow rate of 1l/min and samples were cooled in furnace by switching off the power and maintaining the same flow rate of the hydrogen gas.

Material	Theoretical density [g/cm^3]	pressure [MPa]					
		350		500		700	
		green density and total porosity after pressing					
		ρ [g/cm^3]	P [%]	ρ [g/cm^3]	P [%]	ρ [g/cm^3]	P [%]
MAS1	8,14	6,56	16,05	6,8	13,27	7,02	5,75
MAS2	8,05	6,48	16,39	6,71	15,61	6,77	6,13
MAS3	7,98	6,37	17,25	6,63	14,88	6,73	5,63

Table 2. Green density and total porosity of the compacted samples.

Material	pressure [MPa]								
	350			500			700		
	ρ [g/cm^3]	P [%]	ΔV[%]	ρ [g/cm^3]	P [%]	ΔV[%]	ρ [g/cm^3]	P [%]	ΔV[%]
MAS1	6,55-6,85	15,42-19,12	0,4-3,14	6,68-6,98	13,81-16,9	0,65-4,67	7,22-7,58	6,4-10,85	0,21-3,91
MAS2	6,48-6,7	16,51-19,25	0,75-2,9	6,52-6,78	15,51-18,75	1,02-2,91	7,18-7,45	7,16-10,52	1,15-4,47
MAS3	6,38-6,5	18,01-19,52	1,4-2,32	6,5-6,71	15,36-18,01	1,49-3,5	7,44-7,52	5,14-6,15	1,95-4,61

Table 3. Sintered density, total porosity and volumetric dimensional change for sintered compacts.

After cooling, the samples were polished and chemically etched in order to investigate the microstructure and the porosity by optical microscopy. The green density of the samples compacted at specified pressures and the theoretical density of the three compositions are shown in table 2. After sintering at temperatures and maintaining times mentioned above the iron base compacts achieve densities, porosities and volumetric dimensional change as presented in table 3.

2.2 Dimensional changes

Volumetric diffusion and viscous flow of the matter are the dominant processes that govern linear and volumetric dimensional changes during sintering. Fundamentally admitting the sintering process is materialized by the growth and consolidation of the grain contact, the shrinkage results as a sintering law. But this phenomenon does not always accompany the sintering in all cases obligatorily, very often the opposite occurrence being noticed. There are multitudes of explanations given to this event. Because it cannot always occur simultaneously and with the same intensity in all the material mass the initial approach of the grains, one to each other, causes as expected tensile stresses in some regions. Although in as-isolated domains the material undergoes the compaction by grain closeness and porosity reduction, yet globally the material volume can grow. Tensile stresses might originate as a result of a non simultaneous annihilation of the residual stresses caused by the compacting operation or as a result of a non simultaneous thermal dilatation, a non homogeneous distribution of the grain size or a varying repartition of the compacting pressure. Gases enclosed through the pressing process and those resulted from oxides reduction or emanate from protection atmosphere are sometimes collected in closed pores carrying out pressures on the adjacent material and thus majoring the volume of the pores.

Additionally, swelling process can be observed in those systems where reciprocal diffusion markedly exhibits the Kirkendall effect, which is associated with different diffusion rates of the atoms, or where the liquid phase rapidly diffuses in the solid phase or in those systems where evaporation-condensation process plays an important role (Domsa, 1966).

After sintering the specimens were measured in order to investigate linear and volumetric modifications. During sintering both swelling and shrinkage of the samples were detected, but the most predominant occurrence was swelling of the samples sintered at all three temperatures. The characterization of the sintering behaviour in the presence of the liquid phase was performed by analyzing the influence of the sintering temperature and chemical composition (fig. 1) on the dimensional change of the iron-copper based samples compacted at 350 MPa, 500 MPa and 700 MPa and sintered for 50 min.

The following plots are given on the basis of a predictive modelling and data analysis of the sintering process using Statistica software in order to reach the optimum correlation between sintering parameters and chemical composition for an antifriction material. Swelling of the sintered compacts can be observed at all temperatures for all three compacting pressures. The lower expansion corresponds to all samples sintered at 800°C with a minimum value for the sample containing 1 wt% Sn and compacted at 700 MPa

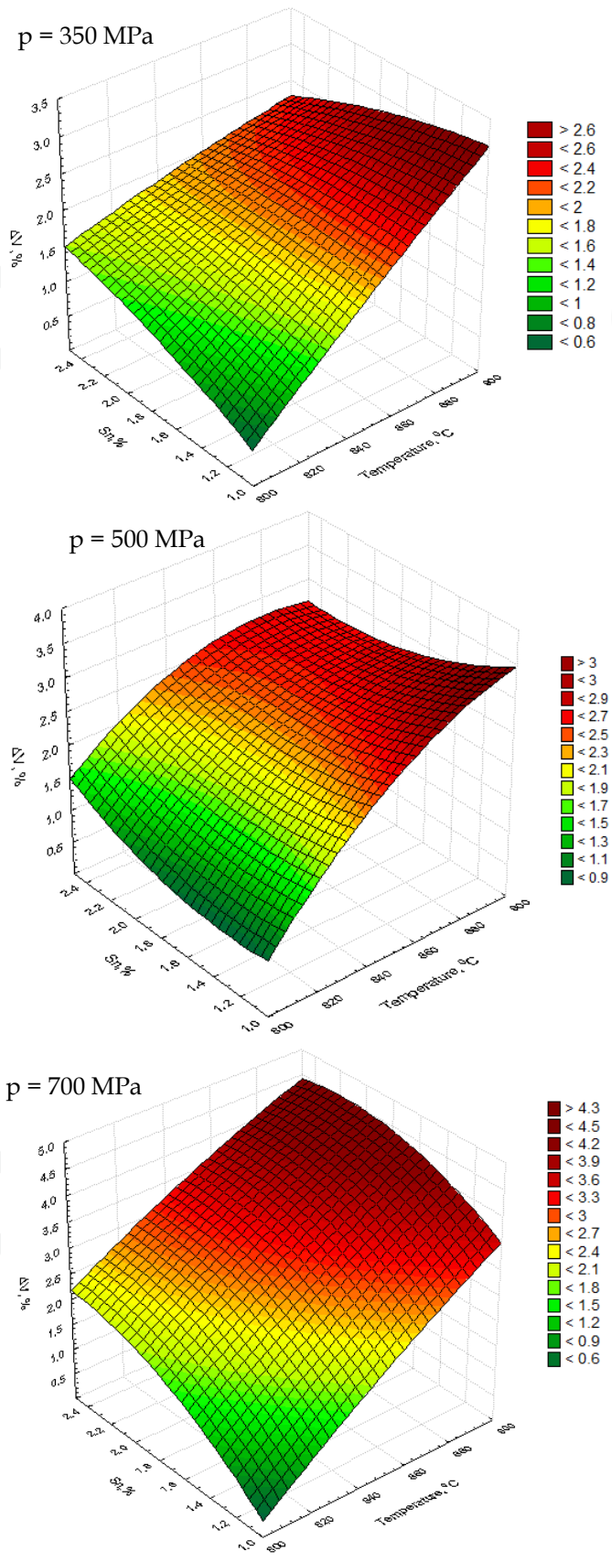

Fig. 1. The effect of tin content and sintering temperature on dimensional changes.

(0,21%). Also, the higher dimensional growth was recorded for all samples sintered at 900°C, the maximum value being detected for the sample compacted at 700 MPa and with a content of 2.5 wt% Sn (4,38%).

A sharper rise of dimensional growth is observed for specimens with a higher starting porosity, particularly at high sintering temperatures. From the plotted graphs almost the same variation of the dimensional changes with tin content is noticed, except for specimens sintered at 900°C and compacted at 700 MPa.

Taking into account that, for copper-tin alloys, the initial melting temperature (solidus) sharply decreases with rising of the tin content, from 1083°C for copper to 798°C for an alloy with 13,2% Sn (Sorokin, 1966), then molten copper-tin will exist in larger quantities and penetrate the solid iron boundaries. Liquid penetration of the grain boundaries causes grain separation and swelling on liquid formation. This penetration action pushes more solid particles apart, increasing the distance between particle centres and consequently leading to the growth of the compacts (Wang, 1999). This behaviour is attributed probably to the formation of Cu-Sn, Fe-Cu and Fe-Sn compounds in larger amounts at higher temperatures as the tin content increases. Diffusion of copper into the iron particles leads to dimensional growth (Sands & Shakespeare, 1966, as cited in Chandrasekaran & Singh, 1996a), and formation of the copper tin alloy along the neck regions in the Fe-Sn intermetallic network also contributes to swelling (Watanabe et al., 1988; Watanabe & Kim, 1984, as cited in Chandrasekaran & Singh, 1996a). The extent of interconnecting pores in the compacts is increased by the formation of the Fe-Sn intermetallic compound, which thus results in compact swelling. Compact swelling due to pore formation at prior particle sites is observed if the liquid particles have substantial solubility in the solid during heating (Lee & German, 1985; Xydas & Salam, 2006, as cited in German et al., 2009). Decreasing of the dimensional changes is attributed to the formation of the Fe-Sn phase at higher temperatures, which has a lower coefficient of thermal expansion than iron (Watanabe & Kim, 1984, 1987, as cited in Chandrasekaran & Singh, 1996b). Another cause of the dimensional growth might be attributed to the trapped hydrogen in the pores as the sintering process was performed in hydrogen atmosphere. Unlike solid coarsening, where volume is conserved, gas-filled pores change volume as they grow since the internal pressure depends on the inverse of the pore size. Thus, as the pores grow the gas pressure decreases and the pore volume increases both due to coalescence and due to the declining pressure, resulting in long-term swelling (German et al,, 2009). The internal pressure in the pore increases with temperature, leading to compact swelling (German & Churn, 1984, as cited in German, 2009). Pore growth occurs in liquid phase sintering due to gas diffusion in the liquid, partially due to annihilation of the smaller pores, but also due to vapour production during sintering (German et al., 2009).

2.3 Total porosity

When the liquid is soluble in the solid swelling occurs, and it is most useful in forming porous structures, such as self-lubricating bearings. Therefore, a great attention should be devoted to the porosity of the compacts for a better description of the sintering process when a liquid phase forms. 3D surface plots from figure 2 show the total porosity of the samples with different tin content compacted at 500 MPa and sintered at 800, 850 and 900°C for 20, 35 and 50 min.

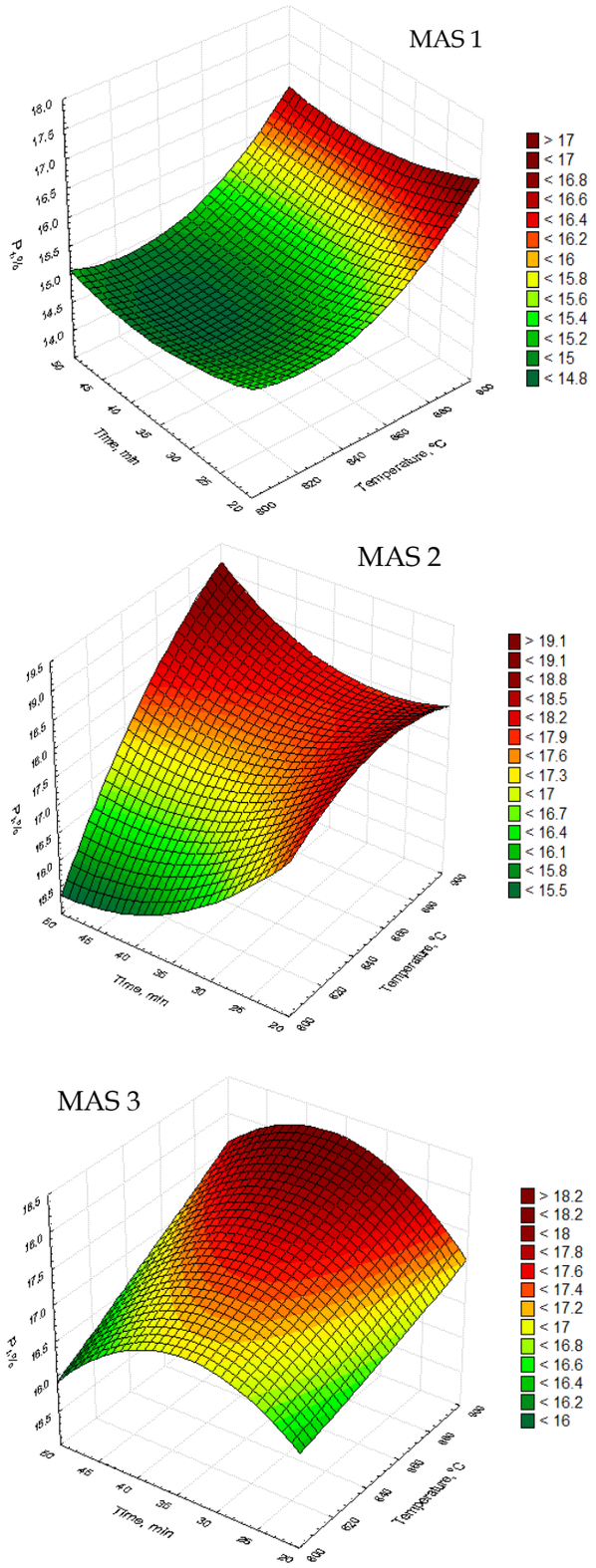

Fig. 2. The effect of sintering time and temperature on total porosity.

From these graphs a non uniform variation of the total porosity with sintering temperature and time can be seen for all three compositions. Samples with 1% tin addition (MAS1) show the same variation of the total porosity at all sintering temperatures. First, a slightly increase of the porosity occurs, up to 35 minutes of maintaining time and then total porosity decreases in the same manner for further sintering time. For samples containing 2,5% Sn (MAS3) a dissimilar tendency can be noticed comparatively with those previously mentioned. As for specimens with 1,5% Sn (MAS2), there is a decreasing in the total porosity as the sintering time is longer for heating at 800°C and 850°C, while sintering up to 50 minutes at 900°C produces a continuous increase of the porosity.

Decreasing of the porosity level is probably due to the formation of the soft phases of Cu-Sn, Fe-Sn-S or Pb-Sn-S, which diffuse into the pores. Capillarity drives the liquid to fill smaller pores prior to greater ones (Shaw, 1993, as cited in German, 2009). As the smaller pores fill, the mean pore size increases while the porosity and the number of pores decrease. Usually, during liquid phase sintering porosity is decreasing, but since smaller pores are annihilated first the mean pore size increases while the grain size is increasing (German et al., 2009).

The formation of a copper-tin alloy at the neck of the iron-tin intermetallic compound generates the initial increase of the porosity and thus restricting diffusion of low melting phases lead, lead-tin or sulphides into the network to fill the pores. Since the diffusion coefficient of copper in tin is higher than that of tin in iron at a temperature of about 850°C, the occurrence of iron-tin intermetallics contribute to the increase in intercommunicating porosity, and in that way increasing total porosity (Watanabe & Kim, 1984, 1987, as cited in Chandrasekaran & Singh, 1996b). Meanwhile, the excess copper surrounding the iron-copper combines to form a copper-tin liquid phase which diffuses into the iron-copper skeleton. Regarding the excess of lead amount, it is possible for this to migrate at the surface of the component forming a soft cover over the hard matrix of iron-copper (Watanabe & Iwatsu, 1980, as cited in Chandrasekaran & Singh, 1996a).

Microscopic investigation of the porosity was performed on the polished and un-etched sample surfaces made from selected compositions compacted at 500 MPa and sintered in the range of 800-900°C for 20 to 50 minutes. Figures 3 through 5 illustrate the optical micrographs for the as-sintered microstructure of MAS1, MAS2 and MAS3 showing the lower and the higher level of porosity for each one.

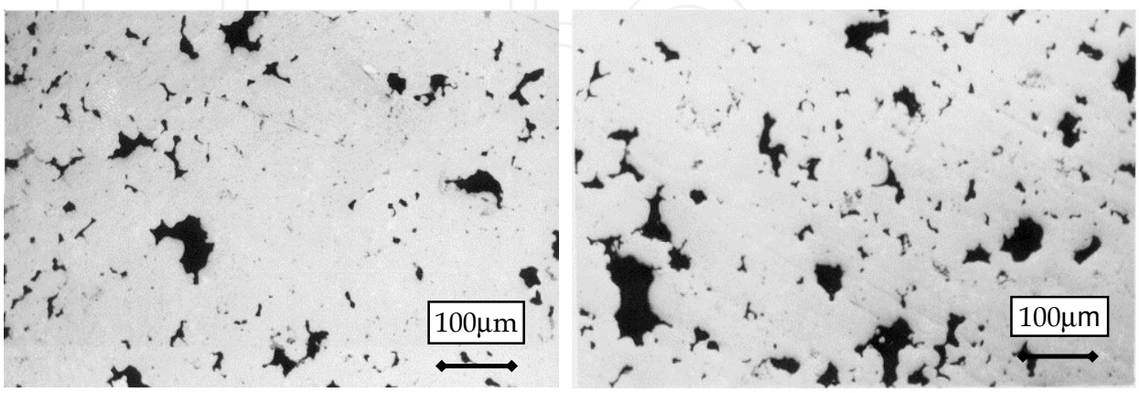

a) b)

Fig. 3. Micrographs showing the porosity of the composition with 1 wt% Sn (MAS1) sintered at: a) 800°C for 35 minutes (13,8%) and b) 900°C for 20 minutes (17,5%).

Figure 3(a) shows some pores of relatively smaller size and few larger pores but both types with predominant irregular shapes and sharp edges or needle-like shapes, and an overall non-uniform distribution. In figure 3(b) the number of the larger pores increases, the majority having the same irregular shape except for few pores with rounded shape. In the same time the distribution of the pores becomes little more uniform.

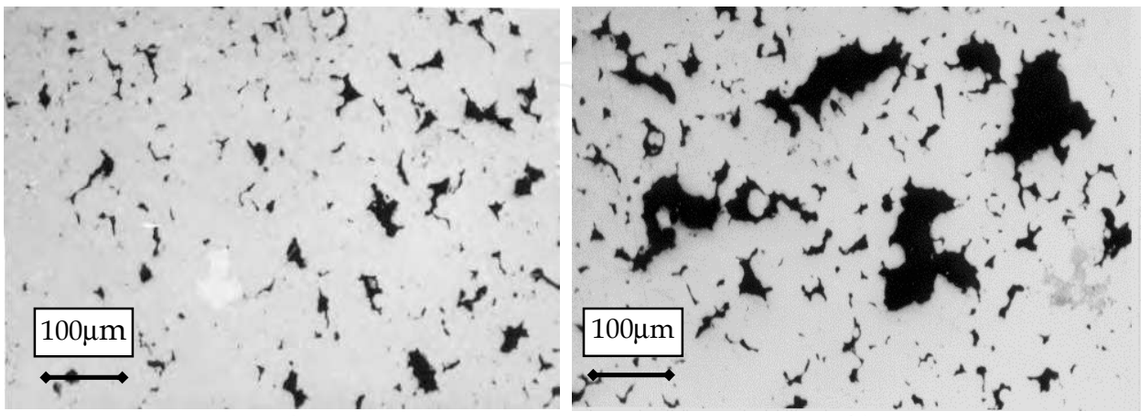

a) b)

Fig. 4. Micrographs showing the porosity of the composition with 1,5 wt% Sn (MAS2) sintered at: a) 800°C for 50 minutes (15,2%) and b) 900°C for 50 minutes (18,7%).

Figures 4 (a) and 4 (b) present a higher degree of porosity with irregular and sharply edged pores of different sizes. In the left micrograph, figure 4 (a), the number of large pores is decreased, and a more uniform distribution can be noticed. A similar distribution of the pores is also observed in the right micrograph, figure 4 (b), still few much larger pores exist.

Microstructure of MAS3, figures 5 (a) and (b) exhibits the highest level of porosity with finer and smaller pores than previous microstructures. Although some agglomeration of pores still exists, the overall repartition of the pores is more homogeneous. Some large pores can be remarked in the sample sintered at 900°C, with irregular shape, but acicular and spot-like shape, even spherical one, are the most predominant profiles of the pores. From the above micrographs it is obvious that pore coarsening occurs at higher sintering temperatures.

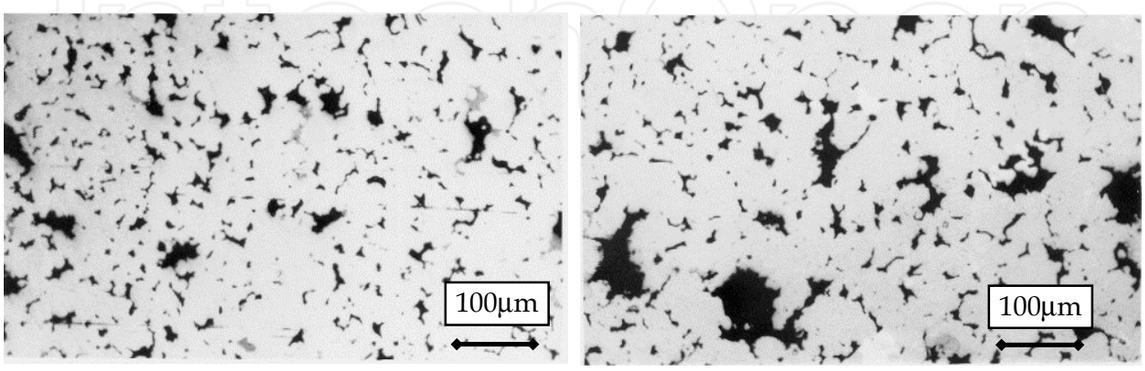

a) b)

Fig. 5. Micrographs showing the porosity of the composition with 2,5 wt% Sn (MAS3) sintered at: a) 800°C for 50 minutes (15,4%) and b) 900°C for 35 minutes (18,0%).

2.4 Microstructure

Representative microstructures developed during sintering in the presence of the liquid phase for the selected compositions are presented in figures 6, 7 and 8.

The liquid-phase sintering starts from a non equilibrium condition involving mixed powders of differing composition. The compact swelling during sintering with a liquid phase is mainly attributed to the boundary penetration of solid particles by the liquid phase (Wanibe et al., 1990, as cited in Wang, 1999).

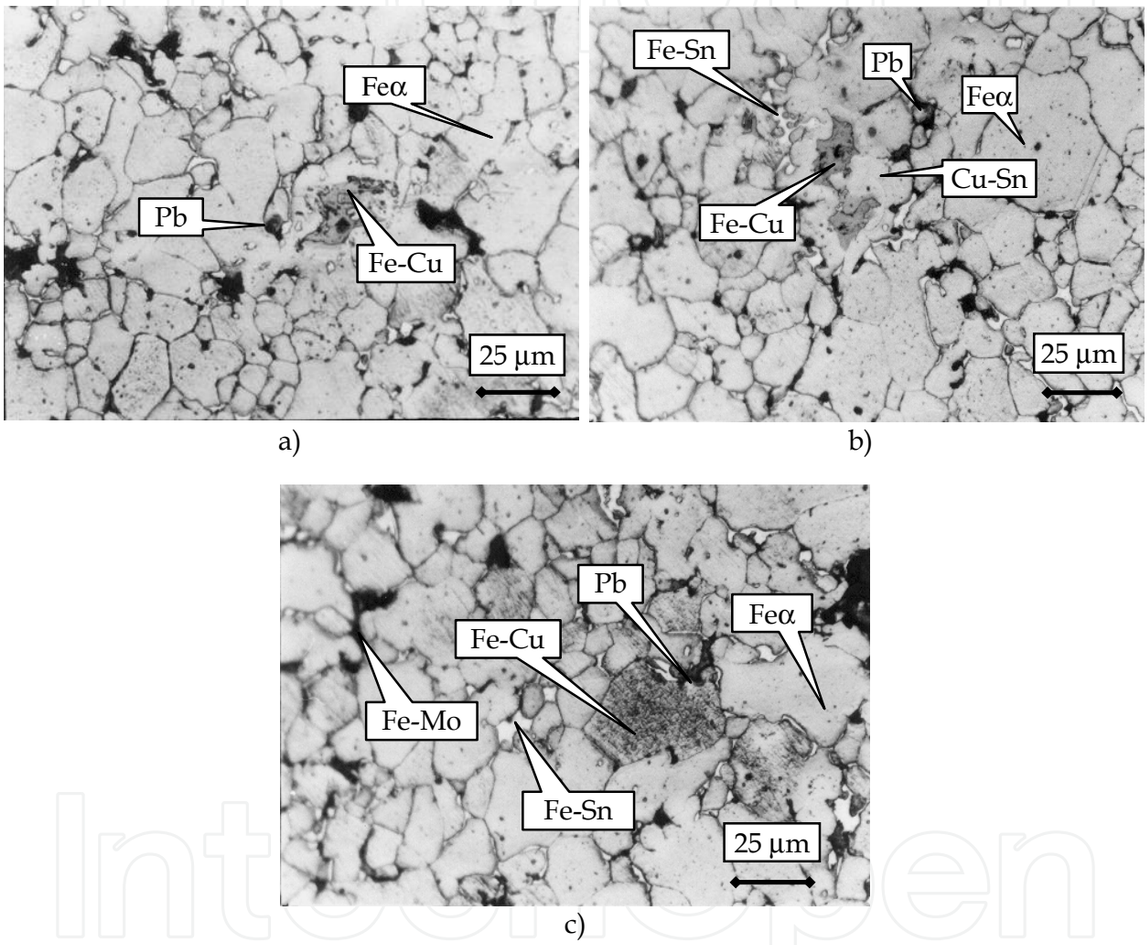

Fig. 6. Microstructure of the MAS1 sintered at: a) 800°C, b) 850°C, c) 900°C for 50 minutes.

Figure 6 shows the microstructure of the iron based samples with 1% Sn, 7,5% Pb and 1% MoS_2 sintered at 800°C, 850°C and 900°C for 50 minutes and emphasize a relatively uniform distribution of the phases with distinctive grain boundaries. Few globular Pb grains and Fe-Cu grains in a ferrite matrix are present in all three microstructures as well as some small pores with irregular shape. In addition, some Fe-Sn and Cu-Sn intermetallic compounds can be seen in the sample sintered at 850°C and few Fe-Mo grains in the sample sintered at 900°C. The microstructure of MAS2 composition (1,5% Sn) sintered at 800°C for 50 minutes (fig.7, a) shows a homogeneous distribution of elongated Fe-Sn grains scattered in the αFe

matrix, Fe-Cu grains and few globular Pb grains. In figure 7 (b) the microstructure of MAS2 alloy is sintered at 850°C for 50 minutes and illustrates the presence of Fe-Cu grains, Fe-Sn grains, Fe-Mo and also few globular Pb grains distributed in the ferrite matrix. The microstructure from figure 7 (c) corresponds to MAS2 composition sintered at 900°C for 50 minutes and exhibits a uniform distribution of the Fe-Sn grains around the neck of the ferrite grains. Also, few elongated Pb grains, Cu-Sn and Fe-Cu grains are detected.

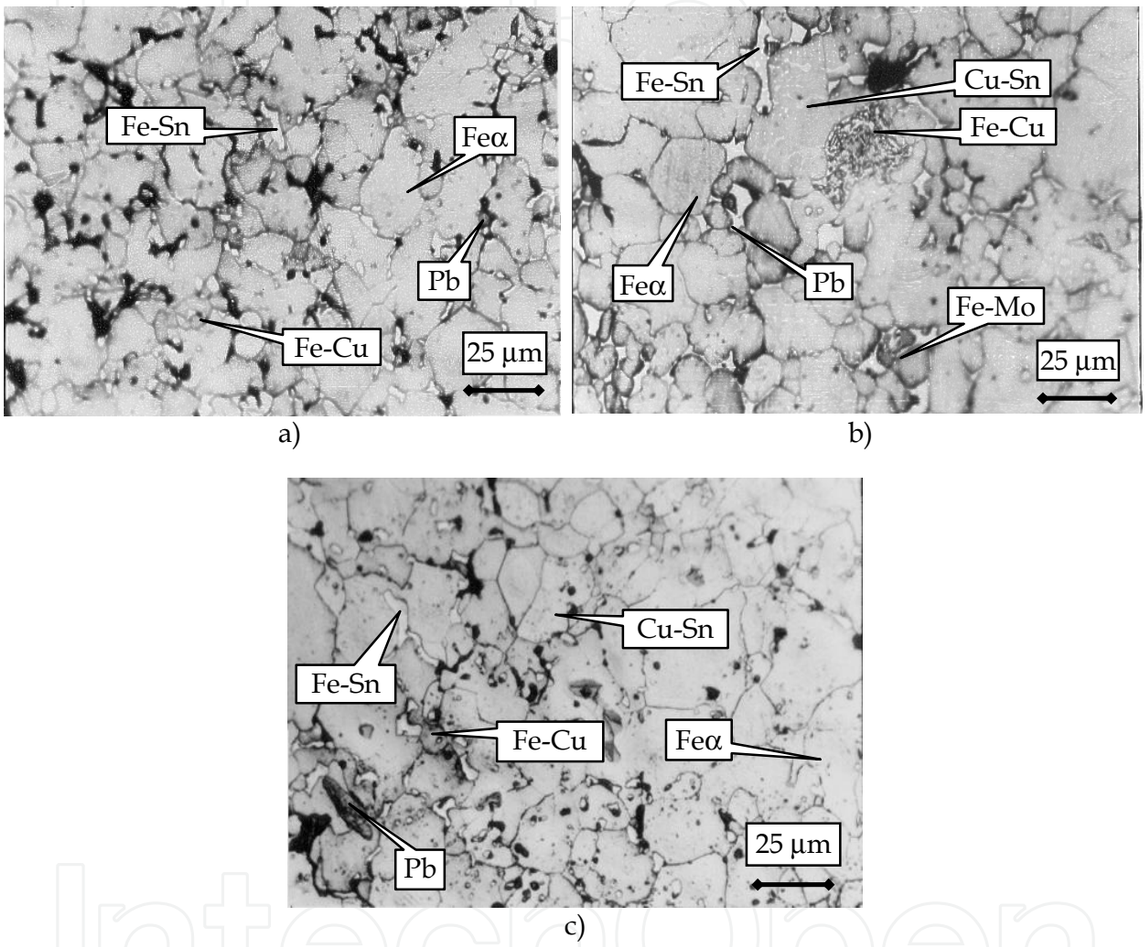

Fig. 7. Microstructure of the MAS2 sintered at: a) 800°C, b) 850°C, c) 900°C for 50 minutes.

Many irregular and small pores can be seen in both samples sintered at 800°C and 900°C placed mainly at the grain boundaries. A large rounded pore can be observed in the sample sintered at 850°C where, prior to its formation, a Cu-Sn grain existed. Large particles generate pores when they form a liquid and when the compact has a low porosity, thus, liquid spreading leads to swelling, but further densification is achieved in longer times (Lu et al., 2001, as cited in German et al., 2009). The sample with 2,5% Sn sintered at 800°C for 50 minutes (fig. 8, a) shows a well-distribution of Fe-Sn grains around the ferrite grains with few spheroidal Pb grains and Fe-Cu grains. Microstructure of the alloy with 2,5% Sn sintered at 850°C contains Fe-Cu and Cu-Sn grains embedded in a Fe-Sn grains network. Also, some globular Pb grains are spotted. The sample with the same composition sintered

at 900°C for 50 minutes contains Fe-Sn grains in a uniform distribution over the αFe skeleton and some Pb, Fe-Cu and Fe-Mo grains. Again, a large pore forms where the tin grains were prior to melting.

From these microstructures it can be observed the liquid formation and a progressive growth of the larger grains at the expense of the smaller ones, giving a fewer grains with a larger average size.

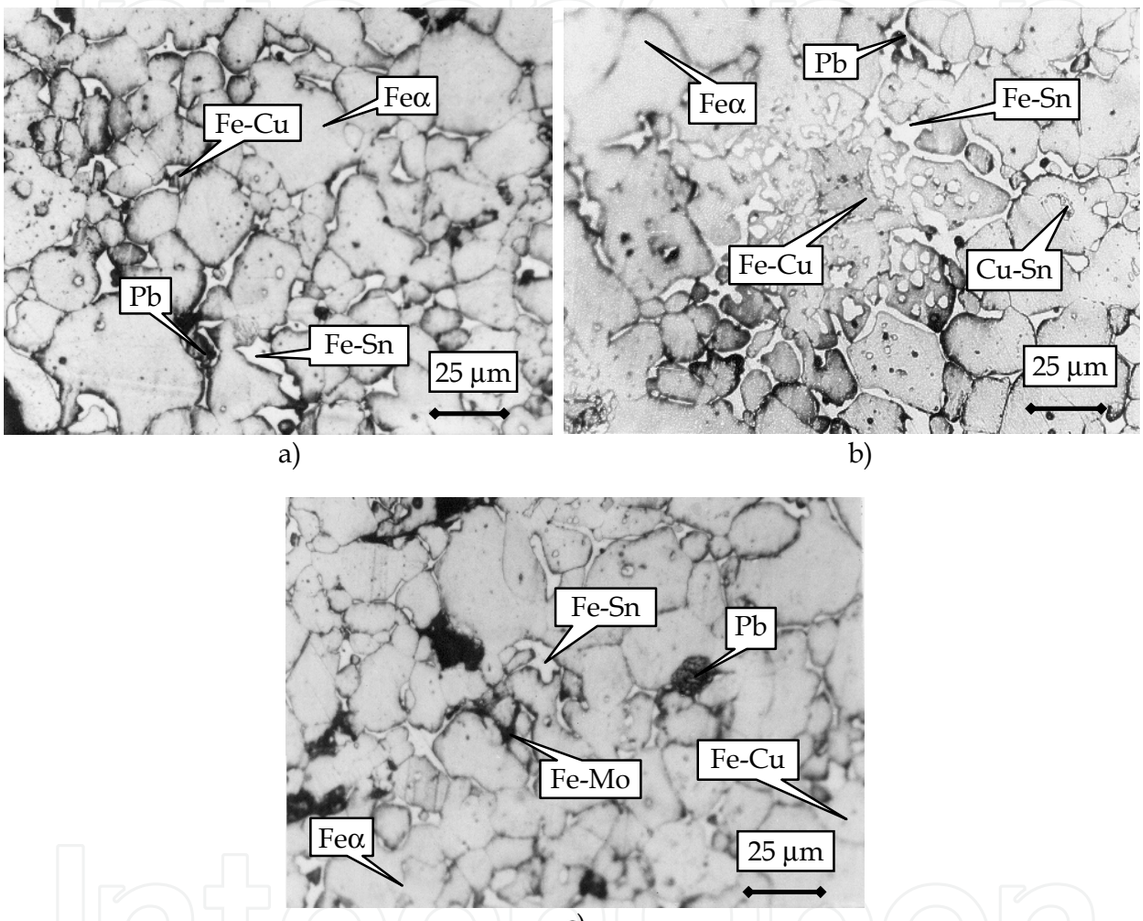

Fig. 8. Microstructure of the MAS3 sintered at: a) 800°C, b) 850°C, c) 900°C for 50 minutes.

Material is transported from the small grains to the large ones by diffusion through the liquid. The liquid spreads and penetrates grain boundaries. After liquid spreading between grains, the film often decomposes into lens-shaped regions forming a necklace microstructure. This occurs because of the increasing surface energy which accompanies completion of a reaction across the solid-liquid interface (German, 1996). This event can be observed on the higher magnification of the optical micrograph shown in figure 9 (a).

The low solubility of the solid copper phase in the liquid lead and tin phase correlated with high solubility of the liquid tin in the solid iron and copper produces the swelling of the system due to decreasing of the liquid volume.

Tin powder particles completely melt and form liquid pools. The liquid phase penetrates the particle boundaries, which possess higher free energy. Figure 9 (b) shows the sample sintered at 800 °C, in which the tin-base liquid phase further penetrates into the grain boundaries of the solid Fe-Cu.

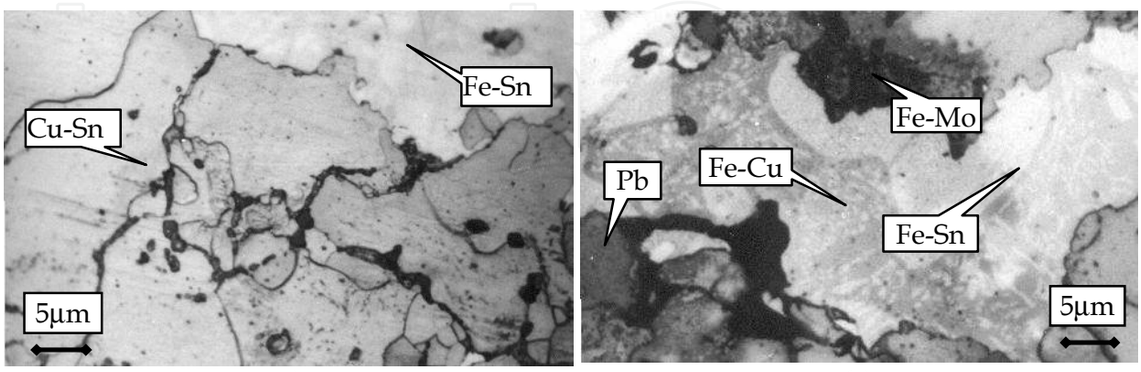

a) b)

Fig. 9. Microstructure of the MAS3 (a) sintered at 850°C/20min and MAS2 (b) sintered at 800°C/50min.

Microstructure coarsening continues and residual pores enlarge if they contain trapped gas, giving compact swelling. Generally, properties of most liquid-phase sintered materials are degraded by prolonged final-stage sintering, thus, short sintering times are preferred in practice (German, 1996). The initial melt induces swelling due to liquid tin and lead penetrating grain boundaries. Pores form at the prior Sn and Pb particle sites. As the Fe particle size increases, swelling goes through a peak. At large sized Fe particles there are fewer interparticle regions for tin base liquid penetration, thus less swelling is observed. Other representative higher magnification microstructures are presented in figure 10.

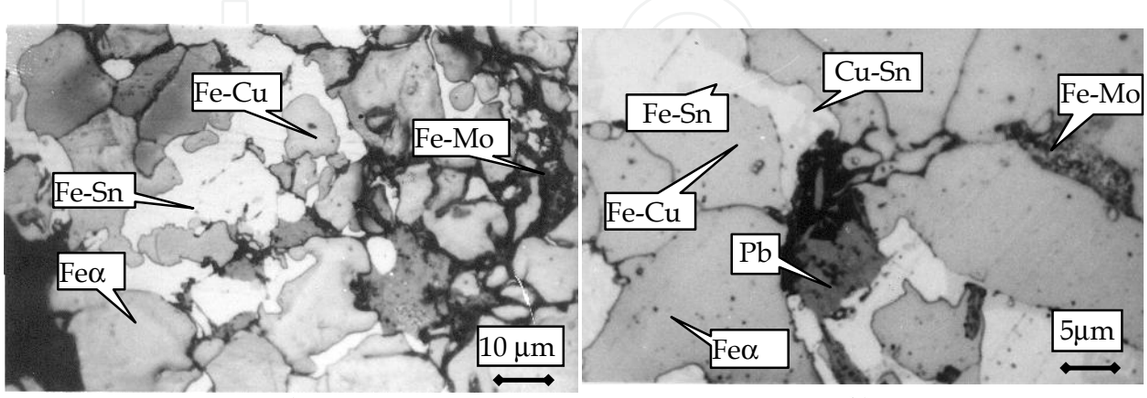

a) b)

Fig. 10. Microstructure of the MAS1 (a) sintered at 800°C/20min and MAS2 (b) sintered at 850°C/50min.

3. Mathematical modelling of the sintering process

A technological process optimization is based on a mathematical model and, generally, it is characterized by two types of parameters or variables: independent parameters (input data) and dependent parameters (output data) (Taloi et al., 1983). The essential target in resolving an optimization problem is to choose the performance or optimization function of the analyzed process. Development of the mathematical models using statistical methods lays emphasis primarily on the concordance between data and the mathematical model, which can be performed by regression analysis (Gheorghe & Ciocardia, 1987). Empirical methods of the mathematical modelling used in regression analysis through passive experiment are based on statistical analysis of the experimental results obtained by varying independent parameters at different levels, intuitively established on previous experiment. The accuracy of the methods increases with the number of the experiments (Micu & Mihoc, 1987). A different situation appears when statistical methods are used in all stages of the experiment: before the experiment by establishing the number of experiments and their performing conditions; during the experiment by processing the results; after the experiment by conclusions referring to development of future experiments. This new way of treating the problem is named "active experiment" and assumes the programming of the experiment (Marusciac, 1973) as follows:

- Establishing the necessary and sufficient number of experiments and their operating conditions;
- Determining the regression equation by statistical methods, which fairly approximate the model of the process;
- Determining the conditions to attain the optimum value of the process performance.

For statistical analysis of the experimental data the sintered density values of MAS1, MAS2 and MAS3 alloys are presented in Table 4. Of a great importance in resolving the optimization problems using the programming of the experiment is to know the influence factors which represent the independent variables.

Temp. [°C]	800°C			850°C			900°C		
Time [min]	20	35	50	20	35	50	20	35	50
Compacting pressure [MPa]	500								
ρ_s	MAS 1								
	6,8	6,98	6,84	6,94	6,73	6,94	6,68	6,83	6,73
ρ_s	MAS 2								
	6,56	6,78	6,8	6,6	6,61	6,56	6,56	6,56	6,52
ρ_s	MAS 3								
	6,59	6,54	6,71	6,64	6,56	6,54	6,54	6,5	6,55

Table 4. Sintered density values for selected materials.

The parameters that influence the sintering process were considered to be sintering temperature, time and lead content. In the regression analysis by active experiment the non-compositional program was used.

3.1 Process performance and variables

The process performance or optimization function proposes to establish the relationship between the density of the powder metallurgy iron-copper based alloys having different additional elements, which refers as a dependent variable, and the sintering process parameters (temperature and time) as well as the lead content, which represent the independent variables.

For the development of the non-linear mathematical model of the sintering process the non-compositional program uses a matrix of experiments. The technological process can be approached by a two degree polynomial function (1), where the dependent parameter (y) is density and the independent parameters (x_1, x_2, x_3) are sintering temperature, maintaining time and lead content.

$$y = b_0 + b_1x_1 + b_2x_2 + b_3x_3 + b_{12}x_1x_2 + b_{23}x_2x_3 + b_{13}x_1x_3 + b_{11}x_1^2 + b_{22}x_2^2 + b_{33}x_3^3 \quad (1)$$

A base level will be established for each variable (independent parameter), which actually represents factorial space coordinates of the starting points. Also, variation ranges (steps) Δz_i will be defined. The superior level is obtained by adding the variation range to the base level and the inferior level is found by extracting the variation range from the base one. If x_i is the codified value of the variable z_i, and is determined from the following relation:

$$x_i = \frac{z_i - z_{0i}}{\Delta z_i} \quad (2)$$

then the superior level will be marked with "+1", the inferior level with "-1" and the base level with "0".

Variable	Sintering temperature		Maintaining time		Lead content	
	natural units, °C	codified values	natural units, min	codified values	natural units, %	codified values
Base level	$z_0 = 850$	$\frac{850-850}{50} = 0$	$z_0 = 35$	$\frac{35-35}{15} = 0$	$z_0 = 5$	$\frac{5-5}{2,5} = 0$
Variation range	$\Delta z = 50$	-	$\Delta z = 15$	-	$\Delta z = 2,5$	-
Superior level	900	$\frac{900-850}{50} = +1$	50	$\frac{50-35}{15} = +1$	7,5	$\frac{7,5-5}{2,5} = +1$
Inferior level	800	$\frac{800-850}{50} = -1$	20	$\frac{20-35}{15} = -1$	2,5	$\frac{2,5-5}{2,5} = -1$
Random value	920	$\frac{920-850}{50} = +1,4$	30	$\frac{30-35}{15} = -0,3$	4,5	$\frac{4,5-5}{2,5} = -0,2$

Table 5. Correspondence between natural and codified units of the variable levels.

Table 5 shows the correspondence between natural and codified units of the independent variable considered in the sintering process optimization: temperature, time, Pb content.

Therefore, the codified notations of the three variables levels are:

x = +1 – Upper level (z_1 = 900°C; z_2 = 50 min.; z_3 = 7, 5%Pb);
x = 0 – Base level (z_1 = 850°C; z_2 = 35 min.; z_3 = 5%Pb);
x = -1 – Lower level (z_1 = 800°C; z_2 = 20 min.; z_3 = 2, 5%Pb).

The variation step for the tin content is different for the three levels and for this reason to establish the optimization function the lead content was considered.

The programming matrix of the experiment is presented in Table 6.

Exp.	Variables													ρ [g/cm³]
	x_0	x_1	x_2	x_3	$x_1 x_2$	$x_1 x_3$	$x_2 x_3$	x_1^2	x_2^2	x_3^2	T[°C]	t[min]	%Pb	
1	+1	+1	+1	0	+1	0	0	+1	+1	0	900	50	5	6,52
2	+1	+1	-1	0	-1	0	0	+1	+1	0	900	20	5	6,56
3	+1	-1	+1	0	-1	0	0	+1	+1	0	800	50	5	6,8
4	+1	-1	-1	0	+1	0	0	+1	+1	0	800	20	5	6,56
5	+1	+1	0	+1	0	+1	0	+1	0	+1	900	35	7,5	6,83
6	+1	+1	0	-1	0	-1	0	+1	0	+1	900	35	2,5	6,5
7	+1	-1	0	+1	0	-1	0	+1	0	+1	800	35	7,5	6,98
8	+1	-1	0	-1	0	+1	0	+1	0	+1	800	35	2,5	6,54
9	+1	0	+1	+1	0	0	+1	0	0	+1	850	50	7,5	6,94
10	+1	0	+1	-1	0	0	-1	0	+1	+1	850	50	2,5	6,54
11	+1	0	-1	+1	0	0	-1	0	+1	+1	850	20	7,5	6,94
12	+1	0	-1	-1	0	0	+1	0	+1	+1	850	20	2,5	6,64
13	+1	0	0	0	0	0	0	0	0	0	850	35	5	6,61
14	+1	0	0	0	0	0	0	0	0	0	850	35	5	6,61
15	+1	0	0	0	0	0	0	0	0	0	850	35	5	6,61

Table 6. The matrix of the second degree non-compositional experiment programming.

3.2 Statistical validation of the regression equation

The experimental error (dispersion of the results reproducibility), s_0^2, is determined with the following formula (3):

$$s_0^2 = \frac{\sum_{u=1}^{n} (y_u - \overline{y})^2}{n-1} \tag{3}$$

u – experiment number
n – number of the experiments
$\overline{y}$ - the average of the results obtained in n parallel experiments

The coefficients of the regression equation (1) are calculated with relations (4) and (5):

For linear effects

$$b_i = \frac{\sum_{u=1}^{N} x_{iu} \cdot y_u}{\sum_{u=1}^{N} x_{iu}^2} \tag{4}$$

For interacting effects

$$b_{ij} = \frac{\sum_{u=1}^{N} x_{iu} \cdot x_{ju} \cdot y_u}{\sum_{u=1}^{N} \left(x_{iu} \cdot x_{ju}\right)^2} \tag{5}$$

The values of these coefficients are statistically evaluated using the relation (6):

$$\left|b_i\right| \geq \left|\Delta b_i\right| \tag{6}$$

$$\left|\Delta b_i\right| = t_{\alpha,N} \cdot s_{b_i} \tag{7}$$

$t_{\alpha, N}$ – Student criterion for α significance level and N degrees of freedom;
s_{bi} – mean square deviation for calculation of b_i coefficient:

$$s_{bi} = \pm\sqrt{s_{bi}^2} \tag{8}$$

s_{bi}^2 – dispersion for calculation of b_i coefficient:

$$s_{bi}^2 = \frac{s_0^2}{\sum_{u=1}^{N} x_{iu}^2} \tag{9}$$

The hypothesis of the model concordance is verified using Fischer criterion (10):

$$F_c = \frac{s_{conc}^2}{s_0^2} \tag{10}$$

s^2_{conc} – calculated model dispersion
s_0^2 – results reproducibility dispersion

The calculated model is concordant when

$$F_c < F_{0,05;\nu 1;\nu 2} \cdot$$

ν_1 – number of degrees of freedom to calculate s^2_{conc}: $\nu_1 = N - k'$
ν_2 – number of degrees of freedom to calculate s^2_0: $\nu_2 = n - 1$

The coefficients of the regression equation that established the link between process performances (sintered density) and independent variables (sintering temperature, maintaining time and lead content) and also the statistical verifying of the regression equation were performed using Maple software:

b0 := 18.21431; b1 := -2.27833; b2 := -.04472; b3 := .154167; b11 := -.0033; b22 := -.022;
b33 := .00266; b12 := .16; b13 := .0122; b23 := .001

3.3 Sintering process optimization

Using statistical analysis of the experimental data regression equations were obtained for independent variables as functions of two and three input data (dependent variables). For analysis of the mathematical models adequacy a multiple regression analysis was performed in order to investigate the errors introduced by mathematical models comparatively with experimental results. For an accurate description of the investigated process using regression analysis, different scale order of the variables possibly causing difficulties for some algorithms should be considered. If the typical values of the problem variables are known, then the problem can be transformed so all variables will have the same scale order. Therefore, it is imperative to have similar scale order for all variables in the interest region and thus, providing a "weight" compensation of all variables during the optimization process. The mathematical models of the density as a function of sintering temperature, maintaining time or lead content (wt%) are presented in table 7, considering two of these input data as independent variables and the third remaining constant.

Input data			Mathematical models
Dependent Variables		Independent Variables	
Pb [wt%]	2.5	Temperature (T_S) Maintaining time (t_S)	$\rho = 11.382 - 1.073T_S + 0.0287t_S + 0.06T_S^2 - 0.007T_St_S + 0.004t_S^2$
	5		$\rho = 16.489 - 2.56T_S + 0.967t_S + 0.16T_S^2 - 0.093T_St_S - 0.022t_S^2$
	7.5		$\rho = -1.769 + 2.045T_S + 0.192t_S - 0.127T_S^2 + 0.003T_St_S - 0.03t_S^2$

Table 7. Mathematical models of the density as a function of two independent variables.

Also, it is very important for final density analysis of the self-lubricating bearings to study the mathematical model of the dependent variable (density) as a function of all three independent variables (temperature, time, chemical composition). This mathematical model is given by the following equation (11):

$$\rho = 18.21431 - 2.72833T_S - 0.04472t_S + 0.154167C_{Pb} - 0.0033T_St_S - 0.022T_SC_{Pb} + 0.00266t_SC_{Pb} + 0.16T_S^2 + 0.0122t_S^2 + 0.01C_{Pb}^2 \quad (11)$$

For an accurate analysis of the process factors influences on the independent variable the results of the statistical analysis are depicted in figures 11 through 13. The 3D graphic

representations show the dependence of the density on two input parameters (sintering temperature and maintaining time) for each of the three compositions (the lead content is considered constant).

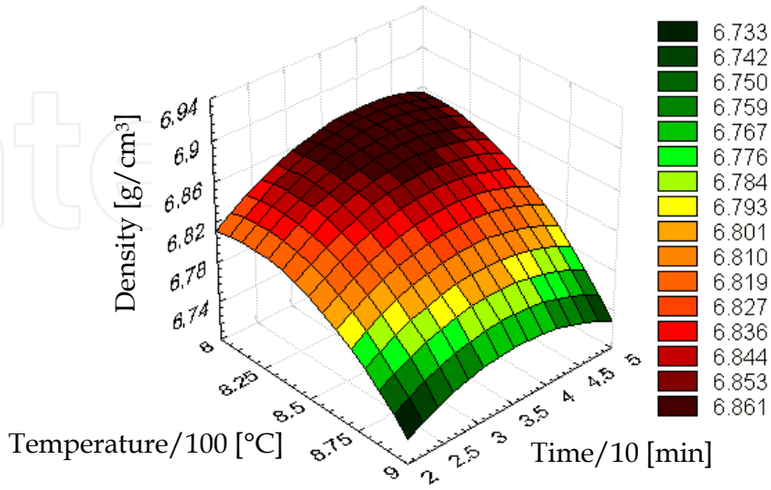

Fig. 11. The dependence of the density on sintering temperature and maintaining time (2.5wt% Pb).

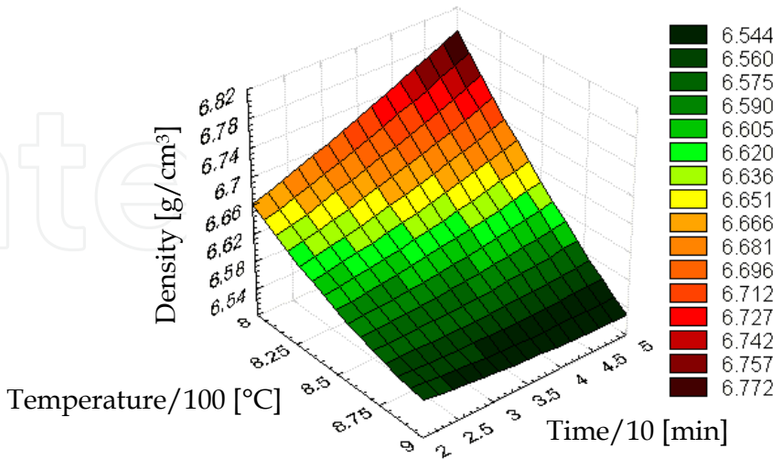

Fig. 12. The dependence of the density on sintering temperature and maintaining time (5wt% Pb).

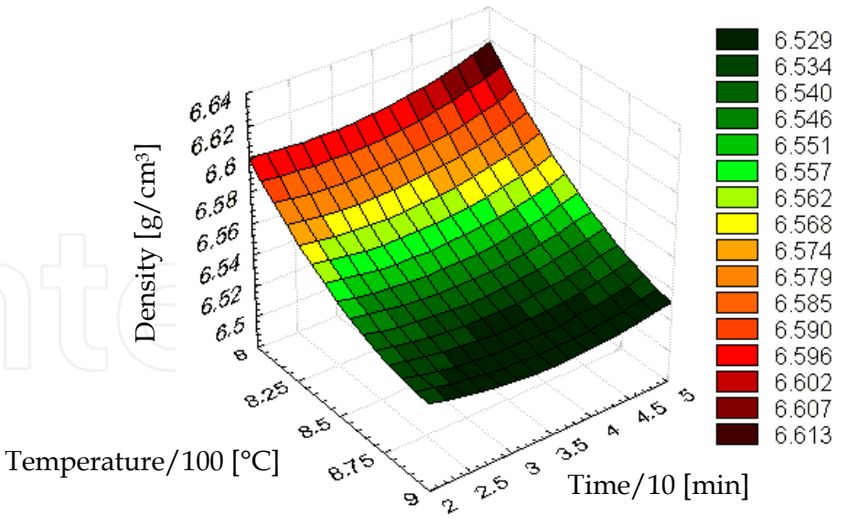

Fig. 13. The dependence of the density on sintering temperature and maintaining time (7.5wt% Pb).

MULTIPLE REGRESSION RESULTS:

Dependent Variable: rho
Multiple R: .96304871
Multiple R-Square: .92746282
Adjusted R-Square: .90767995
Number of cases: 15
F(3, 11) = 46.88212 p < .000001
Standard Error of Estimate: .49053156
Intercept: 7.311416667 Std.Error: .2998758 t(11) = 24.381 p < .000

STAT. MULTIPLE REGRESS.	Regression Summary for Dependent Variable: rho R= .96304871 R^2= .92746282 Adjusted R^2= .90767995 F(3,11)=46.882 p<.00000 Std.Error of estimate: .04905					
N = 15	BETA	St. Err. of BETA	B	St. Err. of B	t(11)	p-level
Intercept			7.311417	.299876	24.38148	.000000
T_s	-.304351	.081205	-.130000	.034686	-3.74793	.003221
t_s	.181440	.081205	.025833	.011562	2.23434	.047166
%Pb	.895496	.081205	.076500	.006937	11.02756	.000000

Table 8. Multiple regression analysis for the dependence of the density on three variables.

The variables estimation coefficients and the residual values were determined by multiple regression analysis of the density dependence on sintering temperature, maintaining time and lead content and the results of these analyses are presented in table 8.

The residual values offer information about errors introduced by using mathematical models comparing with the results obtained by experimental study. These errors represent the difference between the experimental data and analytical data.

The figures 14, 15 and 16 show the relationship between the experimental and calculated values of the density in accordance with the mathematical model, between the residual values and experimental densities and between residuals and calculated densities.

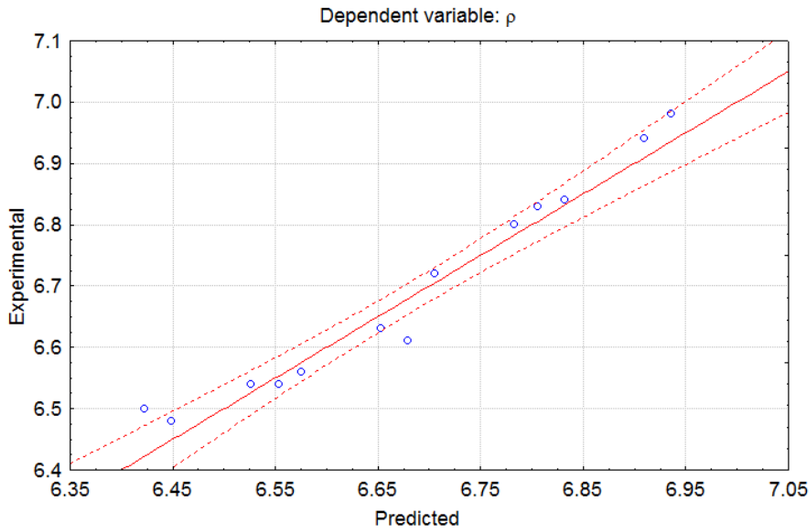

Fig. 14. The dependence between experimental and calculated values of the density.

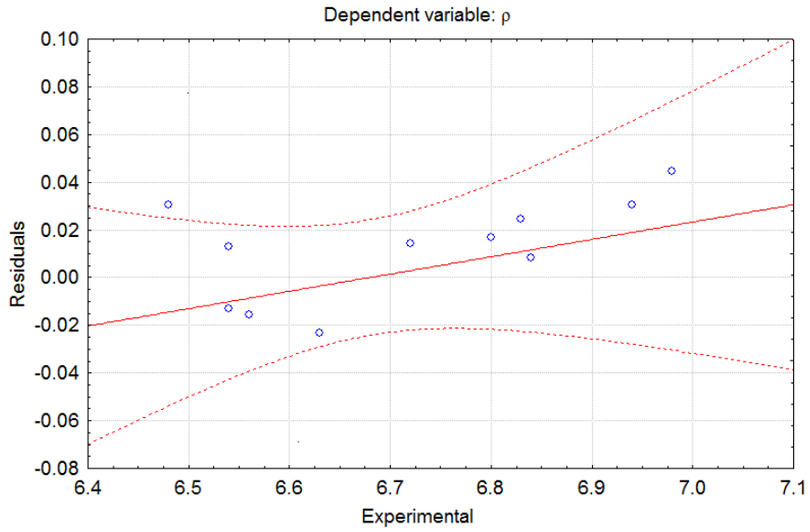

Fig. 15. The dependence between the residuals and experimental values of the density.

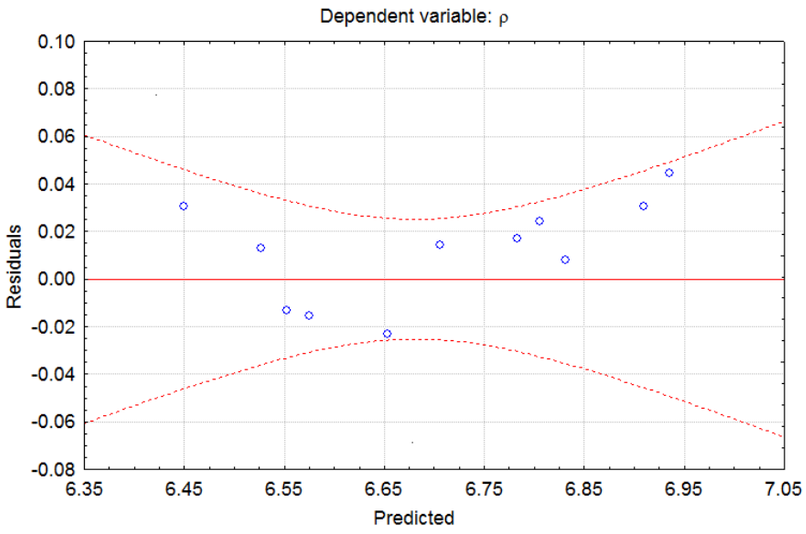

Fig. 16. The dependence between the residuals and calculated values of the density.

4. Conclusions and future research

Using powder metallurgy technologies new Fe-Cu-Sn-Pb materials were developed for tribological applications where the material porosity plays an important role for an adequate functioning of the machines and devices by permitting the retention of a sufficient oil amount in the part pores. Besides the advantages that additions of copper, lead and tin bring to tribological and mechanical properties of self lubricating bearings, these additions direct to the formation of the liquid phase during sintering process causing swelling of the sintered compacts due to pore formation.

From the investigations and observations regarding dimensional changes, total porosity and microstructure development of the iron-copper based alloys with different addition elements during sintering in dry hydrogen atmosphere at 800°C, 850°C and 900°C, the following remarks are drawn:

- Due to high solubility of the liquid in the solid, formation of a transient liquid phase of Sn is observed. Considering the sintering temperature and tin content, swelling of all samples sintered under specified conditions was observed. Lower values of the dimensional change were noticed for the sample with 1 wt% Sn compacted at 700 MPa and sintered at 800^0C. This decrease of the dimensional change is attributed to the formation of the Fe-Sn phase at higher temperatures, which has a lower coefficient of thermal expansion than iron. A sharper rise of dimensional growth is detected for specimen with 2.5 wt% Sn (4,38%) sintered at 900°C and compacted at 700 MPa, and is due possibly to the formation of Cu-Sn, Fe-Cu and Fe-Sn compounds in larger amounts. The volume expansion behavior can be ascribed to the boundary penetration of solid particles by the tin-base liquid phase. Cu-Sn liquid phase wets the iron skeleton, diffuses into the iron and enhances growth. Also, the dimensional growth might be attributed to the tapped hydrogen in the pores as the sintering process was performed in hydrogen atmosphere;

- A non uniform variation of the total porosity with sintering temperature and time can be seen for all three compositions. Usually, during liquid phase sintering porosity is decreasing, but since smaller pores are annihilated first the mean pore size increases while the grain size increases. The highest value of total porosity was observed for sample with 1,5% Sn sintered at 900°C for 50 minutes and the lowest one was for sample with 1% Sn sintered at 800°C for 35 minutes. This behaviour is attributed to the formation of the soft phases of Cu-Sn, Fe-Sn-S or Pb-Sn, which diffuse into the pores and hence, decreasing total porosity, and to the formation of iron-tin intermetallics which contribute to the increase in intercommunicating porosity, and in that way increasing total porosity. Microscopic investigation of the selected materials porosity shows pore coarsening at higher sintering temperatures. Also, the number of pores increases as the tin content increases, except for the specimen with 1,5% Sn sintered at 900°C for 50 minutes. Few larger pores with main irregular shapes and a non uniform distribution can be identified in all samples. Smaller size pores present an overall homogeneous distribution with acicular and spot-like shape and even spherical;
- Representative microstructures developed during liquid phase sintering show a ferrite matrix with distinctive grain boundaries, but irregular shape and different size. Cu-Sn and elongated Fe-Sn grains are relatively uniformly distributed at the intergranular sites in the ferrite matrix. Also, globular Pb grains, Fe-Cu, some Fe-Cu sulphide and Fe-Mo grains can be found in the ferrite matrix. Many irregular and small pores can be seen in all samples, placed mainly at the grain boundaries, and few large pores where the tin grains were prior to melting, surrounded by molten tin. From these microstructures the liquid formation can be observed and a progressive growth of the larger grains at the expense of the smaller ones gives a fewer grains with a larger average size. Penetration of the solid Fe-Cu particles boundary by the tin base liquid phase generates swelling of the compact. A necklace microstructure forms when the tin liquid between grains decomposes into lens-shaped regions due to the increasing surface energy which accompanies completion of a reaction across the solid-liquid interface.

Mathematical model or the optimization function of the sintering process was developed using statistical methods which lays emphasis primarily on the concordance between data and the mathematical model. Using regression analysis of the density dependence on two independent variables (sintering temperature and time), the third one (lead content) being considered constant, and on three independent variables (sintering temperature, sintering time and lead content), the following conclusions are drawn:

- Mathematical models are sufficiently precise and the errors introduced are no greater than 5%;
- The adequacy of the mathematical model is confirmed by the admissible values of the parameters and coefficients obtained using regression analysis;
- The lead content has the maximum influence on the sintered parts density and then in lessening order, the sintering temperature and the maintaining time;
- The mathematical model can be applied to the sintering processes in order to obtain an optimal relationship between antifriction properties of the self-lubricating bearings, and sintering process parameters and the material composition.

Considering the purpose for which these materials were developed, at this point of the research the alloy containing 2,5% Sn presents the highest level of total porosity among these three materials taken in this study, but its microstructure homogeneity should be improved for a better distribution of the phases and pores into the ferrite matrix with more uniform size and regular shape of grains. To reach this goal further research will be proceed by employing mechanical alloying of elemental powders and microwave sintering for the achievement of nanostructures with unique properties.

5. References

Baranov, N. G., Ageeva, V. S., Zabolotnyi, L. V., Il'nitskaya, A., I., Mokrovetskaya, V. S. & Sabaldyr, V. Ya. (1990). Structure and Properties of the Powdered Antifriction Material Iron-Copper-Tin-Lead, In: *Powder Metallurgy and Metal Ceramics*, Vol.29, No.7, 08.09.2011, Available from: http://www.springerlink.com/content/j73vk6147mp13545/

Boivie, K. (2000). SLS Application of the Fe-Cu-C System for Liquid Phase Sintering, In: *Proceedings of the Solid Freeform Fabrication Symposium*, 03.09.2011, Available from: http://utwired.utexas.edu/lff/symposium/proceedingsArchive/pubs/Manuscripts/2000/2000-18-Boivie.pdf

Chandrasekaran, M. & Singh, P. (1996a), Effect of Pb Additions on the Friction and Ware of Sintered Fe-Cu-Sn-MoS_2, In: *The International Journal of Powder Metallurgy*, Vol.32, No.1, pp. 51-58, ISSN 08887463

Chandrasekaran, M. & Singh, P. (1996b), Effect of Sn on the Properties of Fe-Cu-Pb-MoS_2 Antifriction Alloy In: *The International Journal of Powder Metallurgy*, Vol.32, No.4, pp. 323-330, ISSN 08887463

Domsa, Al. (1966). *Tehnologia Fabricarii Pieselor din Pulberi Metalice (Manufacturing Technology of the Metallic Powder Parts),* Ed. Tehnica, Bucuresti, Romania

German, R., M. (1985). *Liquid Phase Sintering*, Plenum Press, ISBN 0-306-42215-8, New York

German, R., M. (1996). *Sintering Theory and Practice*, John Wiley & Sons, ISBN 0-471-05786-x, New York

German, R., M., Suri, P. & Park, S., J. (2009). Review: Liquid Phase Sintering, In: *Journal of Materials Science,* Vol.44, No.1, 03.09.2011, Available from: http://www.springerlink.com/content/eu8804w248232124/

Gheorghe, M., Ciocardia, C. (1987). *Metodologie de determinare a functiilor de regresie, incluzand variabile independente nesimetrizabile, (Methodology for Determination of the Regression Functions, Including non-symmetrical independent variables),* In: *Bulletin of Polytechnic Institute of Bucharest*, pp. 35-70

Kostornov, A.G. & Fushchich, O. I. (February 2007). Sintered Antifriction Materials, In: *Powder Metallurgy and Metal Ceramics*, Vol.46, Nos.9-10, 02.09.2011, Available from: http://www.springerlink.com/content/9221327246150781/

Kostornov, A.G., Fushchich, O. I. & Chevichelova, T. M. (May 2007). Structurization in Sintering of Antifriction Powder Materials Based on Iron-Copper Alloys, In: *Powder Metallurgy and Metal Ceramics*, Vol.46, Nos.11-12, 02.09.2011, Available from: http://www.springerlink.com/content/7ml73l6r46245576/

Marusciac, I. (1973). *Metode de Rezolvare a Problemelor de Programare Neliniara (Methods for Resolving Non-linear Programming Problems),* Ed. Dacia, Cluj-Napoca, Romania

Micu, N. & Mihoc, Gh. (1987). *Elemente de Teoria Probabilitatilor si Statistica Matematica (Elements of Probabilities Theory and Mathematical Statistics),* Editura Didactica si Pedagogica, Bucuresti, Romania

Shahparast, F. & Davies, B. L. (February 2003). A study of the potential of sintered iron-lead and iron-lead-tin alloys as bearing materials, In: *Ware*, Vol. 50, Issue 1, 24.08.2011, Available from: http://www.sciencedirect.com/science/article/pii/0043164878902521

Sorokin, V. K. (1966). Densification during the Sintering of Copper-Tin Powder Alloys, In: *Powder Metallurgy and Metal Ceramics*, Vol.5, No.11, 03.09.2011, Available from: http://www.springerlink.com/content/x24862v5nmugw681/

Sustarsic, B & Kosec, L. (1998). Engineering Properties of Fe-MoS_2 Powder Mixtures, In: *Proceedings of the 1998 Powder Metallurgy World Congress & Exhibition*, pp. 316-321, ISBN 1-899072-09-8, Granada, Spain, October 18-22, 1998

Takata, J. & Kawai, N. (1995). Dimensional Changes During Sintering of Iron Based Powders, In: *Powder Metallurgy*, Vol.38, No.3 (1995), pp. 209-213

Taloi, D., Florian, E., Bratu, C. & Berceanu, E. (1983). *Optimizarea Proceselor Metalurgice (Optimization of the Metallurgical Processes)*, Editura Didactica si Pedagogica, Bucuresti, Romania

Verghese, R & Gopinath, K. (1989). The Influence of Antimony Additions on Sintered Iron-Copper Bearing Materials, In: *Key Engineering Materials*, Vol. 29-31, P. Ramakrishnan, (Ed.), pp. 457-464, Trans. Tech. Publications, ISBN 978-0-87849-577-1, Switzerland

Wang, W.-F. (1999). Effect of Tin Addition on the Microstructure Development and Corrosion Resistance of Sintered 304L Stainless Steel, In: *Journal of Materials Engineering and Performance*, Vol.8, No.6, 31.08.2011, Available from: http://www.springerlink.com/content/w772221x0w030u28/

Yusof, F., Hameedullah, M. & Hamdi, M. (2006). Optimization of Control Parameters for Self-lubricating Characteristics in a Tin Base Composite, In: *Engineering e-Transaction, University of Malaya,* 31.08.2011, Available from: http://ejum.fsktm.um.edu.my/article/346.pdf

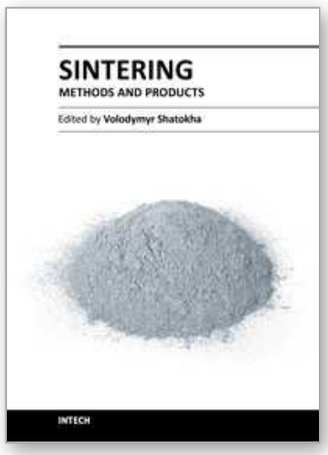

Sintering - Methods and Products

Edited by Dr. Volodymyr Shatokha

ISBN 978-953-51-0371-4
Hard cover, 316 pages
Publisher InTech
Published online 23, March, 2012
Published in print edition March, 2012

This book is addressed to a large and multidisciplinary audience of researchers and students dealing with or interested in sintering. Though commonly known as a method for production of objects from fines or powders, sintering is a very complex physicochemical phenomenon. It is complex because it involves a number of phenomena exhibiting themselves in various heterogeneous material systems, in a wide temperature range, and in different physical states. It is multidisciplinary research area because understanding of sintering requires a broad knowledge - from solid state physics and fluid dynamics to thermodynamics and kinetics of chemical reactions. Finally, sintering is not only a phenomenon. As a material processing method, sintering embraces the wide group of technologies used to obtain such different products as for example iron ore agglomerate and luminescent powders. As a matter of fact, this publication is a rare opportunity to connect the researchers involved in different domains of sintering in a single book.

InTech Europe
University Campus STeP Ri
Slavka Krautzeka 83/A
51000 Rijeka, Croatia
Phone: +385 (51) 770 447
Fax: +385 (51) 686 166
www.intechopen.com

InTech China
Unit 405, Office Block, Hotel Equatorial Shanghai
No.65, Yan An Road (West), Shanghai, 200040, China
中国上海市延安西路65号上海国际贵都大饭店办公楼405单元
Phone: +86-21-62489820
Fax: +86-21-62489821

IntechOpen